Robust 4D-MRI Sorting with Reduced Artifacts Based on Anatomic Feature Matching

by

Zi Yang

Graduate Program in Medical Physics
Duke University

Date: _____
Approved:

_____
Jing Cai, Co-Supervisor

_____
Lei Ren, Co-Supervisor, Chair

_____
Fang-Fang Yin

_____
Robert E. Reiman Jr.

Thesis submitted in partial fulfillment of
the requirements for the degree of
Master of Science in the
Graduate Program in Medical Physics
in the Graduate School of
Duke University

2018

ABSTRACT

Robust 4D-MRI Sorting with Reduced Artifacts Based on Anatomic Feature Matching

by

Zi Yang

Graduate Program in Medical Physics
Duke University

Date: _____
Approved:

_____
Jing Cai, Co-Supervisor

_____
Lei Ren, Co-Supervisor, Chair

_____
Fang-Fang Yin

_____
Robert E. Reiman Jr.

An abstract of a thesis submitted in partial
fulfillment of the requirements for the degree of
Master of Science in the
Graduate Program in Medical Physics
in the Graduate School of
Duke University

2018

Abstract

Purpose: Motion artifacts induced by breathing variations are common in 4D-MRI images. This study aims to reduce the motion artifacts by developing a novel, robust 4D-MRI sorting method based on anatomic feature matching, which is applicable in both cine and sequential acquisition.

Method: The proposed method uses the diaphragm as the anatomic feature to guide the sorting of 4D-MRI images. Initially, both abdominal 2D sagittal cine MRI images and axial MRI images (in both axial cine and sequential scanning modes) were acquired. The sagittal cine MRI images were divided into 10 phases as ground truth. Next, the phase of each axial MRI image is determined by matching the diaphragm position in the intersection plane between the axial MRI and the ground truth cine MRI. Then, those matched phases axial MRI images were sorted into 10-phase bins identical to the ground truth cine images. Finally, 10-phase 4D-MRI were reconstructed from these sorted axial MRI images. The accuracy of reconstructed 4D-MRI data was evaluated in a simulation study using the 4D eXtended Cardiac Torso (XCAT) digital phantom with a sphere tumor in the liver. The effects of breathing signal, including both regular (cosine function) and irregular (patient data), on reconstruction accuracy were investigated by calculating total relative error (TRE) of the 4D volumes, Volume-Percent-Difference

(VPD) and Center-of-Mass-Shift(COMS) of the simulated tumor between the reconstructed and the ground truth images.

Results: In both scanning modes, reconstructed 4D-MRI images matched well with the ground truth except minimal motion artifacts. The averaged TRE of the 4D volume, VPD and COMS of the EOE phase in both scanning modes were 0.32%/1.20%/$\pm 0.05mm$ for regular breathing, and 1.13%/4.26%/$\pm 0.21mm$ for patient irregular breathing, respectively.

Conclusion: The preliminary results illustrated the robustness of the new 4D-MRI sorting method based on anatomic feature matching. This method improved image quality with reduced motion artifacts in the resulting reconstructed 4D MRI is applicable for axial MR images acquired using both cine and sequential scanning modes.

Contents

List of Tables

List of Figures

Acknowledgements

I would like to express my gratitude to my advisors Dr. Jing Cai and Dr. Lei Ren for their insightful mentoring and patient guidance. I would also like to thank the other members of my thesis committee, Dr. Fang-Fang Yin and Dr. Robert E. Reiman Jr., for their time and efforts.

I would also like to appreciate the support, help and inspiration from all the lab mates in Radiation Physics, and classmates and faculty from the Medical Physics Graduate Program.

1. Introduction

1.1 Respiratory Motion in Radiation Therapy

Radiation therapy utilizes ionizing radiation to kill tumors. However, the radiation dose can also cause damage to the surrounding healthy tissues. Thus, one important aspect of radiation therapy is to deliver adequate dose to the target while limiting the dose to the neighboring organs-at-risk (OARs). To achieve this goal, accurate target delineation and inter/intra-fraction motion management are two key factors for a successful image-guided radiation therapy (IGRT) treatment. However, respiratory motion can be an important source of error that induces uncertainties in these aspects [1, 5].

In the imaging step of radiation therapy, respiratory motion can cause motion artifacts in the images, which could be expressed as smeared, compressed or discontinuous structures [1]. These artifacts will induce distortion of the target volume and inaccurate positional and volumetric information [2]. In the planning step, these artifacts can further lead to problems about imprecise target delineation, inaccurate dose calculation, and uncertainties in the margin selection. In the treatment delivery, respiration-induced intra-fraction motion can cause variations from the intended dose distribution along the motion path. Overall, respiratory motion could be a potential

error source to cause overdose to OARs and under-dose to the target volume, which will contribute to compromised clinical outcome.

Therefore, respiratory motion management is of significance, especially in the abdominal and thoracic cancers, where the organ and tumor motion is a major component of the treatment uncertainties [3]. Furthermore, for stereotactic body radiation therapy (SBRT), respiratory motion management is specifically a key component considering the smaller target volume and higher prescription dose [4].

1.2 Four-Dimensional(4D) Imaging in Radiation Therapy

Four-dimensional (4D) imaging adds time as the fourth dimension into 3D volumetric images to introduce temporal information, especially the respiratory motion, into the spatial information [2]. Generally, 4D imaging is generated by re-ordering and re-binning the data, whether reconstructed images or raw data, into pre-defined phase bins to reveal clear body respiratory motion during an entire breathing cycle without blurring in the motion path.

The process of 4D imaging can be summarized in 3 key steps:

1) Imaging: Use different imaging tools to obtain raw data.
2) Sorting: Divide the raw data or images into phase bins. Correlate the image data with the motion signal.

3) Reconstruction: Create a digital image the 4D volume based on the sorted data.

In clinical practice, 4D imaging is an essential part of image-guided radiation therapy(IGRT) [7, 8]. Respiratory motion can introduce motion artifacts into images, thus causing uncertainties in patient geometry or anatomic structures. However, 4D imaging can largely eliminate this problem as it provides clear respiratory motion of both organs and tumor, which will allow more accurate target delineation/localization, better margin selection and more accurate 4D dose accumulation [6].

1.2.1 4D Computed Tomography

Currently, the most popular clinical application of 4D imaging technique is 4D Computed Tomography (CT). In clinical practice, 4D-CT is the most commonly used technique to evaluate and manage patient respiratory motion, especially for the lung and abdominal treatment [8,9]. It is widely used for patient-specific treatment planning and the determination of the treatment delivery method. Specifically, 4D-CT is generally used for determining the target volume and margin to account for the respiratory motion induced intra-fraction displacement, and to achieve better and more accurate tumor dose coverage. In addition, 4D-CT provides the electron density of different tissue and structures, which is essential for accurate dose calculation [10]. However, one drawback of 4D-CT is that the low soft-tissue contrast in CT images can cause

uncertainties or errors in abdominal tumor delineation and organ separation. In addition, CT image acquisition involves extra imaging radiation dose. Current 4D-CT operation is commonly in the cine mode or the helical mode, which means a set of projections data is acquired over at least one breathing cycle for each patient volume [11]. Then the data are re-binned or sorted according to a known breathing surrogate. For example, in clinical practice, the Varian Real-time Position Management™ (RPM) system is often applied to provide an external breathing signal for 4D-CT reconstruction. Chest and abdomen CT images can only be acquired in axial mode, which can lead to compromised quality for the visualization of respiratory motion because respiratory motion is more dominant in the SI direction [12].

1.2.2 4D Magnetic Resonance Imaging

Recently, 4D Magnetic Resonance Imaging (MRI) has become an emerging technique for imaging respiratory motion in IGRT. 4D-MRI provides a promising respiratory motion management modality with excellent soft-tissue contrast for tumor delineation with no known radiation hazard to the patients, compared with CT. As is shown in Figure 1, the superior soft-tissue contrast provides benefit to the imaging of

the abdominal region and has shown great utility, especially in pancreatic cancer. [14]

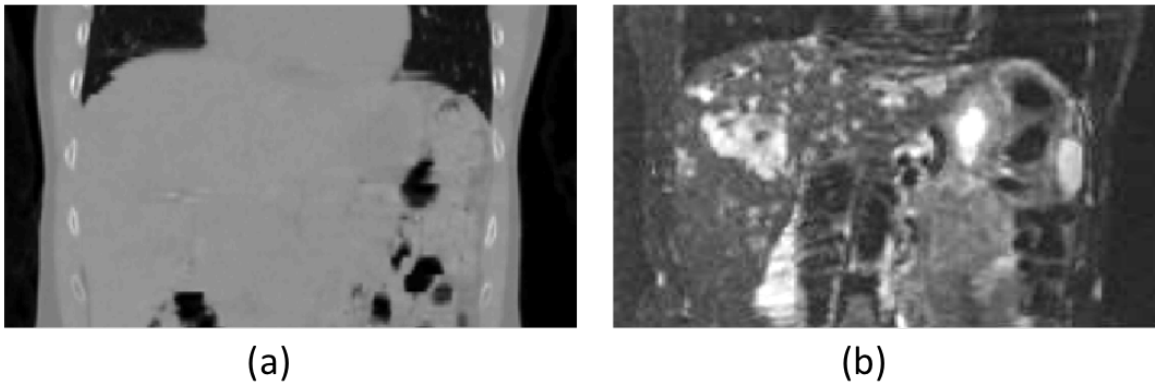

Figure 1: Comparison of same patient's (a) 4D-CT and (b) 4D-MRI at same body region: 4D-CT image shows insufficient soft-tissue contrast while 4D-MRI image indicates different abdominal organs

The non-ionizing radiation dose to the patients permits the feasibility of longer imaging time, imaging during the treatment, and daily imaging capability, which will allow improved motion management and target verification. In addition, compared with CT image slices in only the axial orientation, MRI can also allow data acquisition in different planes, as well as 3D volumetric acquisition, which can provide more accurate information about the respiratory motion effects in radiation therapy.

1.3 Current 4D-MRI Technologies

As is discussed in the previous section, 4D-MRI yields promising advantages in respiratory motion management in IGRT. Currently, various reconstruction methods have been proposed and developed for 4D-MRI in different approaches. There are mainly two approaches for the current 4D-MRI techniques.

1.3.1 Prospective 4D-MRI Techniques

The first approach is prospective 4D-MRI technique, which can also be described as dynamic MRI. This technique focuses on the first step of 4D imaging, which is the imaging part, as mentioned before. This approach usually uses a fast 3D pulse sequence with gating to obtain 3D volumetric images at different pre-determined motion amplitudes, or uses a fast 2D sequence to obtain continuous 2D images at different slices with breathing control. For example, Hu et al. proposed a 4D-MRI technique with an amplitude-based triggering system implemented into the standard turbo spin echo (TSE) sequence. [15] However, the use of triggering or gating may often cause long image acquisition time. Although the acquisition duration of this real-time technique is short compared to conventional diagnostic pulse sequence, this approach can only allow limited images to be acquired over one breathing cycle. In addition, there is always a trade-off between fast imaging and high image quality due to technical limitations. For instance, Dinkel et al. developed a 4D-MRI technique using 2D dynamic TrueFISP sequence and 4D TREAT MRI sequence to obtain tumor motion with the frame rate of 0.7 frames/s and the spatial resolution of 3.1x3.1x4mm. [16] Blackall et al. investigated a real-time 4D-MRI technique applying a 3D free-breathing FFE-EPI sequence with SENSE parallel imaging, for which the frame rate is approximately 3 volume/s but the spatial resolution is 1.8x1.8x7mm for the entire lung volume. [17]

1.3.2 Retrospective 4D-MRI Techniques

The second approach is retrospective 4D-MRI technique, in which continuously acquired 2D MRI images are sorted based on different surrogates that reveal the respiratory motion. This technique is mainly focused on the second key step in the 4D imaging process, which is sorting. 2D images are sorted based on corresponding time stamps in a respiratory cycle or are sorted according to the amplitude information of respiration motion into different phase bins. Various retrospective sorting methods for 4D-MRI have been developed. Some of the methods utilize external surrogates, such as biomarkers or RPM signals, to sort the images [18,19]. However, there are still challenges with these methods. For example, the correlation between the external signal and the respiratory motion and its reliability needs to be further verified. The acquisition of an external breathing signal is inconvenient and requires extra configuration in facilities. In addition, the external signal needs to be synchronized with image acquisition [20]. Another method is to utilize internal signals extracted from image features as the surrogate, which shows better validity compared with the previous method [21]. But the extraction of appropriate internal surrogates from imaging process is also challenging. For example, Cai et al. have investigated a sorting technique using body area estimation in 2D slices as the respiratory surrogate [22]. Liu et al. have developed an 4D-MRI sorting method to re-assign 2D MRI images into corresponding phase bins based on

sagittal–coronal–diaphragm point of intersection tracking [23]. Compared to the prospective approach, this approach provides better spatial resolution, but the scanning time is extended.

The retrospective sorting methods can be achieved in both cine acquisition mode and sequential acquisition mode. The cine acquisition mode is demonstrated in Figure 2 [24]. A series of 2D images of one slice are continuously obtained during a period of time. Then it moves to next slice position to acquire a new series of images. This process keeps repeating to cover the whole volume of target.

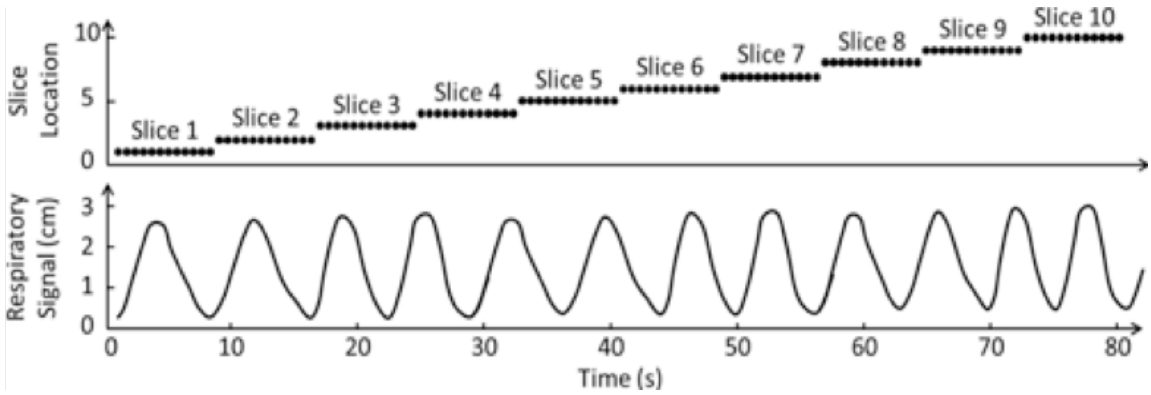

Figure 2: Cine acquisition mode: Continuously acquire images at one slice location for several repetitions then move to next slice location [24]

In contrast to the cine mode, the sequential acquisition mode first acquires images from the first slice position to the last slice position for one time. Then this process repeats from the first slice position again for several times to ensure sufficient respiratory motion information is obtained for every slice location. The scheme of sequential acquisition mode is illustrated in Figure 3 [24].

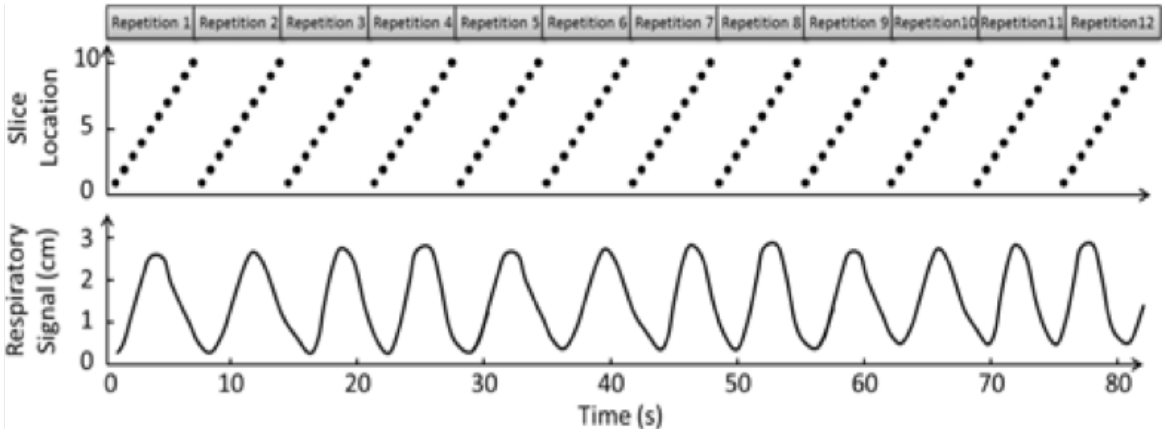

Figure 3: Sequential acquisition mode: Acquire images one slice location by one slice location then start over again for several repetitions [24]

The implementation of these two acquisition modes is largely depend on the imaging techniques and the 4D-MRI sorting methods. The cine mode is often achieved by the TrueFISP/FIESTA pulse sequence. 4D-MRI sorting methods like using body area (BA) as the respiratory surrogate are developed based on the cine mode [22]. The sequential mode is always used in HASTE/SSFSE pulse sequence. Methods like result-driven phase-sorting technique can be integrated into this acquisition mode [25]. Previous study has shown that the cine acquisition mode is more susceptible to

breathing variation compared to the sequential acquisition mode [25]. To achieve the same data completeness, the sequential mode often requires longer scanning time than the cine mode with redundant data acquired. Sequential mode permits the removal of data obtained during irregular breathing periods, while it is not applicable in the cine mode because it causes insufficient information for reconstruction.

1.4 Breathing Variation-Induced Artifacts

As demonstrated in Figure 4 [26], 4D images often exhibit breathing variation induced motion artifacts or the stitching artifact, shown as tissue discontinuities at structure boundaries. This issue is caused by the influence of irregular breathing on the data consistency over the respiratory cycles. A study has investigated the influence of breathing variation in 4D-CT images and found that breathing variation can caused an up to 20% volume reduction in the reconstructed images [27]. It is also found that in 4D-PET images the breathing variation can result in lengthening in the respiratory motion direction [28]. Due to the sampling and resolution limitation as well as breathing variations, motion artifacts are inherent in the 2D image-based retrospective sorting methods. To deal with the motion artifacts, some breathing guidance techniques are used to train the patient to produce relatively regular breathing patterns during the image acquisition. But the effectiveness of the breathing guidance is still limited and may restricted by the patient's medical condition.

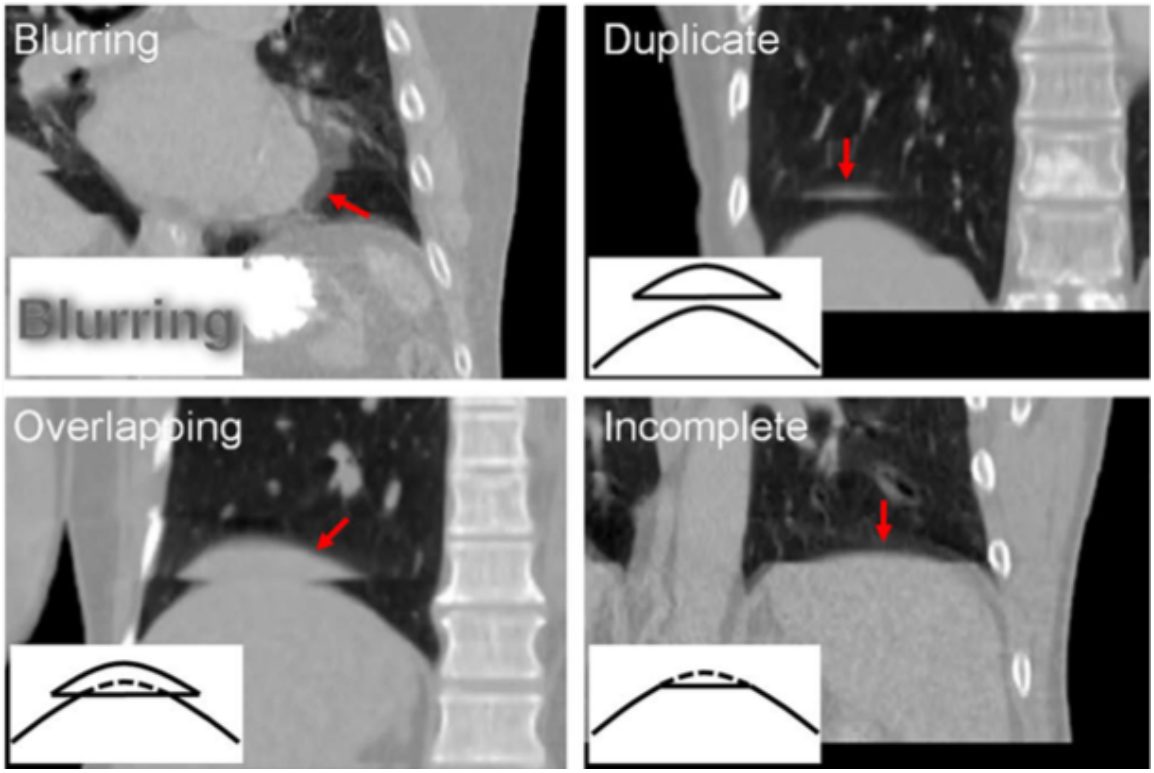

Figure 4: Breathing variation induced motion artifacts in 4D imaging shown as blurring, duplicate, overlapping, incomplete organ structures in the 4D images [26]

1.5 Aims of This Study

Various 4D-MRI techniques have been developed and have shown promising results for clinical applications. These 4D-MRI techniques often assume reproducible breathing patterns; thus, the sorting process will cause the stitching artifact when breathing variation occurs, which presents as the discontinuities of the anatomic structures in the reconstructed 4D-MRI images.

This study aims to develop a robust 4D-MRI sorting method based on anatomic feature matching for motion artifact reduction that can be applied to both cine and sequential acquisitions.

The specific aims can be described as below:

Aim 1: Develop a preliminary anatomic feature matching-based (AFM) 4D-MRI sorting method for both cine and sequential acquisitions.

Aim 2: Investigate the robustness of this method for irregular breathing using both simulated and patient breathing signals.

2. Methods and Materials

2.1 Methods

2.1.1 Workflow of This Study

Figure 5 shows the overall workflow of this anatomic features matching based 4D-MRI sorting method. The general idea is to acquire two groups of orthogonal MRI images, then detect the anatomic features in the two image groups, and finally sort the images into different bins by matching their anatomic features to directly preserve better organ/tissue structure. In this method, we chose the diaphragm as the landmark feature to be detected and matched. The reason for choosing the diaphragm is that first, tumor motion is primarily influenced by the diaphragm motion. Second, the respiratory motion is more dominant in the superior–inferior (SI) direction, which can be captured by the diaphragm. In addition, the diaphragm structure can be easily extracted from images due to the naturally defined border between liver and lung.

This detailed method can be described in the following three steps:

(1) Image acquisition: Two groups of orthogonal scans are acquired in this process. The first group is the single-slice sagittal cine images located at the right diaphragm peak location (where the diaphragm is most superior). They are acquired over several breathing cycles. The second group is the axial slices located at multiple positons acquired over a volume of interest, which is the 4D-MR scan. The acquisition mode of this axial scan can be either cine mode or sequential mode.

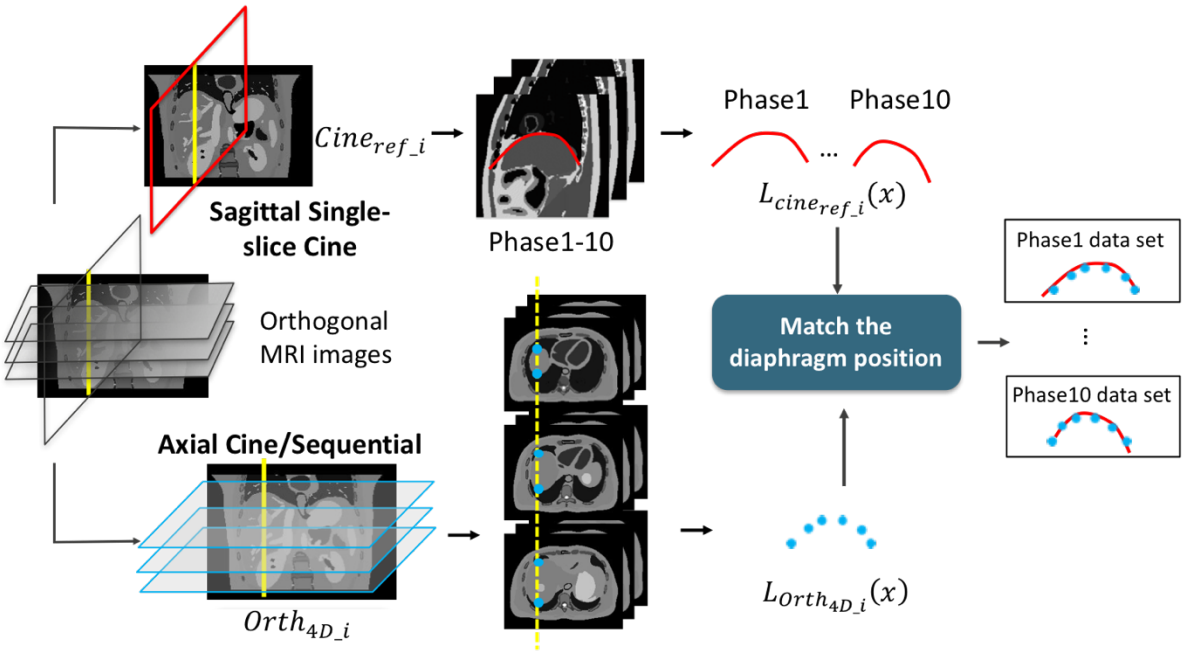

Figure 5: The overall workflow of the anatomic feature matching-based 4D-MRI sorting method

(2) <u>Diaphragm Extraction:</u> The second step is to detect the diaphragm in those two groups of images.

For the sagittal single-slice cine images, 10 reference images representing 10 respiratory phase bins in a breathing cycle are first selected according to the diaphragm motion in the images. Then the diaphragm structures in these 10 sagittal images are extracted by a region-growing based method shown in Figure 6 [32]. This extraction method consists of the following steps:

(a) manual selection of a seed point inside the liver region in the sagittal image., and defining a 9 by 9-pixel matrix around the seed point;

(b) calculation of the image intensity threshold of the liver by averaging the 3 maximum intensity values and 3 minimum intensity values in the matrix to reduce the

influence of noise, then using this threshold to filter the image intensity to be within the liver intensity range;

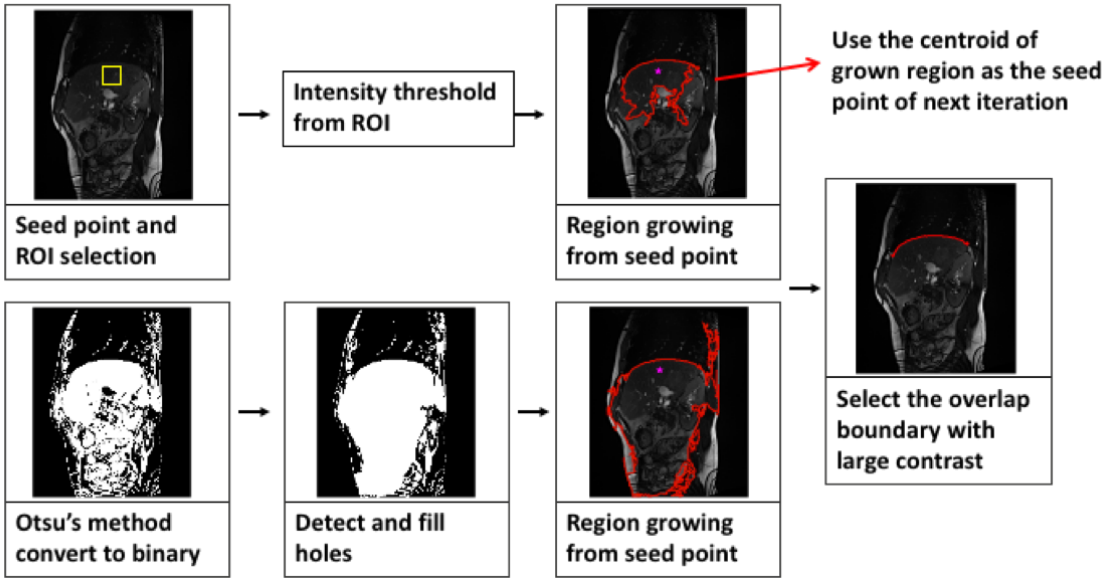

Figure 6: The workflow of extracting diaphragm structures from the sagittal cine MRI images

(c) using the region-growing algorithm to extract the liver boundary by searching image pixels within the threshold starting from the seed point [29];

(d) using Otsu's method to change the image into a binary format [30]. This method will change the body intensity into 1 and change the lung and background intensity into 0, and filling the holes inside the body in the binary image;

(e) using the region-growing algorithm to extract the body boundary by growing from the seed point;

(f) Due to the well-defined natural contrast of the liver and lung, the boundary of diaphragm is clear and accurate in the two boundaries obtained in steps (c) and (e). taking the overlap part of these two boundaries to extract the diaphragm structure;

(g) extracting the diaphragm from next sagittal slice by using the centroid of the grown-region in step (c) as the seed point of next iteration to make the process more automated.

The 10 diaphragm structures extracted from the sagittal images that represent 10 different respiratory bins are used in later steps to guide the sorting process of axial slices.

The diaphragm positions in axial slices are extracted by a peak-valley detection algorithm. The profiles of the intersection line of each axial image and single-slice cine image (Yellow dash line in the Figure 5) are analyzed by a peak-valley detection program to find the boundary point of liver and lung due to the naturally defined contrast of liver and lung. The peak-valley detection program is developed in Matlab (MathWorks, Natick, MA) to find true peaks and valleys in the image line profile by ignoring small local fluctuations caused by imaging noise.

(3) <u>Sorting by diaphragm matching:</u> The sorting process is performed by matching the diaphragm position in the axial images with the 10 reference diaphragm structures extracted from sagittal images and then sort the axial images into the corresponding phase bins. The diaphragm boundary extracted from the sagittal

reference images can be described as $L_{ref_i}(x)$, where i represents the phase bin 1-10. The boundary from the axial slices can be represented as $L_{axial_{4D\_i}}(x)$. The sorting process to get the 3D volume of phase i (which is $4D\_i$) can be considered as finding the axial slice set that can minimize the difference between $L_{axial_{4D\_i}}(x)$ and $L_{ref_i}(x)$. This process can be expressed as:

$$Diff = \sum_{x=1}^{N} \left| L_{axial_{4D\_i}}(x) - L_{ref_i}(x) \right| \quad [1]$$

$$4D\_i = argmin(Diff\left(L_{axial_{4D\_i}}(x), L_{ref_i}(x)\right)) \quad [2]$$

2.1.2 Strategy for sorting Slices Outside the Diaphragm region

The beginning and ending slices in the axial MRI scan may not contain diaphragm structures. To sort those slices, this diaphragm matching method can be combined with other sorting methods to assign into their corresponding bins. In this method, these out-of-diaphragm images are sorted based on the maximum cross-correlation (CC) of the profiles in the sagittal/axial images at the sagittal-axial intersecting plane (Yellow solid line in Figure 7).

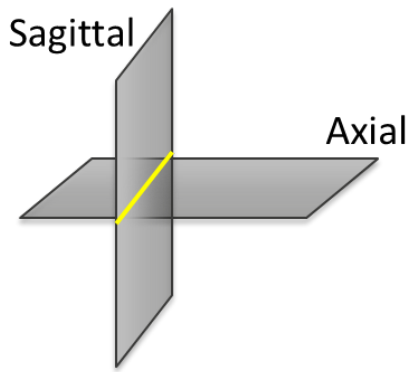

Figure 7: An illustration of the Sagittal-Axial intersecting line profile for sorting the out-of-diaphragm axial images

The cross-correlation can be defined as the formula below:

$$CC = \frac{E((x-\bar{x})(y-\bar{y}))}{\sigma_x \sigma_y} \quad , \qquad [3]$$

where the x represents the pixels of the profile in sagittal image and y represents the pixels of the profile in axial image. E represents the expectation and σ means the standard deviation.

For example, an out-of-diaphragm axial slice can be assigned into phase bin N when:

$$\max\left(CC_{sagi_1}, \dots, CC_{sagi_{10}}\right) = CC_{sagi_N} \quad , \qquad [4]$$

where CC_{sagi_i} means the cross correlation between the axial profile and the sagittal profile of phase i.

2.1.3 Strategy for Empty or Over-Filled Bins

Following the sorting process, every axial slice can be assigned to a certain phase bin corresponding to the diaphragm position.

However, there might be empty bins for a certain phase at certain slice location. To solve this problem, a strategy has been made to first copy the same slice from the phase in opposite slope. If that phase bin is also empty, then copy the slice from adjacent slices in the same phase. If the previous bins are empty, copy the same slice from adjacent phases.

In addition, there might be bins for a certain slice location at a certain phase that are over-filled with multiple images. To solve this situation, a strategy has been made to keep the slice which has the largest sagittal-axial intersecting profile cross correlation of the corresponding phase.

After every slice bin of each phase is filled with only one image, then the ten 3D volumes are reconstructed by combining the axial slices together, and then further reconstructing a 4D volume.

2.1.4 Phase Sorting

For evaluation purposes, the conventional phase sorting method is also applied in every simulation case to further compare with the anatomic feature matching methods [25]. For a known breathing signal, a peak/valley detection is performed to detect every breathing peak during a scan. The interval between two neighboring peaks is regarded as a single respiratory cycle and then is divided into 10 equally-spaced bins. Each image will be assigned into a phase bin if its acquisition time stamp falls into the corresponding bin in that cycle.

The strategy for empty phase bins is same as the anatomic feature matching method. However, for the redundant images in one phase bin, the image acquired at the closest time point to the bin center is kept.

2.2 Materials and Simulation Scheme

2.2.1 Materials

This 4D-MRI sorting technique is developed and investigated using the 4D extended Cardiac Torso (XCAT) digital phantom to simulate the image acquisition and reconstruction [31]. The XCAT digital phantom simulated images in the activity mode with organs' intensity assigned to mimic the T2-Weighted MR images. The liver lesion is set to be 30mm in diameter and to move with liver together during respiration. The respiratory motion of the XCAT digital phantom is controlled by the input breathing signals.

2.2.2 Simulation Scheme

The effects of breathing signals, including both regular and irregular in both axial cine and sequential modes, are simulated and investigated.

2.2.2.1 Regular Breathing Simulation

Cine and sequential scans are simulated with a regular cosine breathing pattern in XCAT digital phantom as shown in Figure 8.

The parameters of the simulated images are set to mimic the real MRI scan:

Resolution: $1.67 \times 1.67 \times 1.67 mm^3$

Frame Rate: $0.3s/frame$

Respiratory rate: $3.1s/cycle$

Maximum Diaphragm Displacement: $3cm$

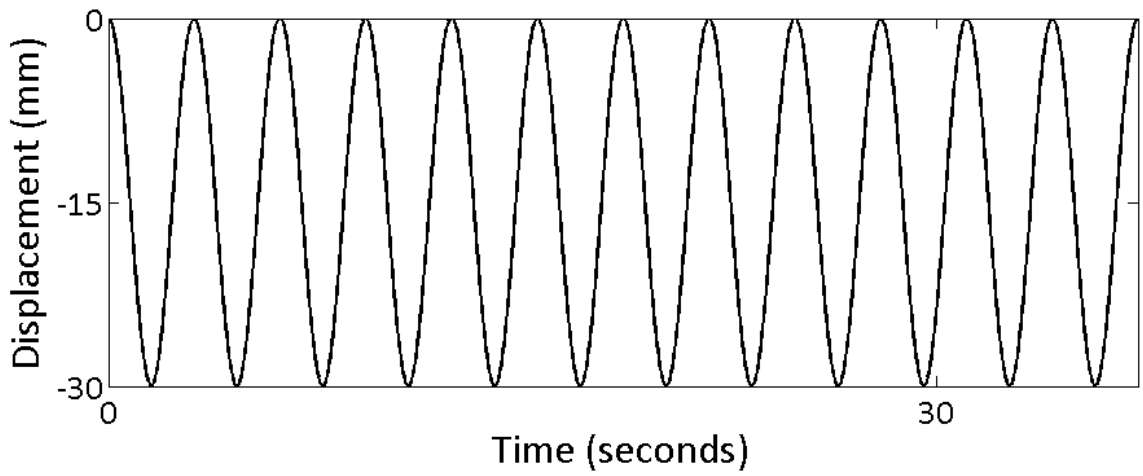

Figure 8: Regular cosine breathing curve used for raw MRI data simulation

2.2.2.2 Irregular Breathing Simulation

Cine and sequential scans with two types of irregular breathing curves (8 curves in total) are simulated in the XCAT digital phantom.

The parameters of the simulated images are set to mimic the real MRI scan:

Resolution: $1.67 \times 1.67 \times 5.00\ mm^3$

Frame Rate: $0.3s/frame$

Maximum Diaphragm Displacement: $3cm$

(1) Simulated irregular signals: 3 types of irregular signals are simulated based on simple cosine signal as is shown in Figure 9: (a) cosine signal with changing periods;

(b) cosine signal with changing amplitudes; and (c) cosine signal with changing periods and amplitudes.

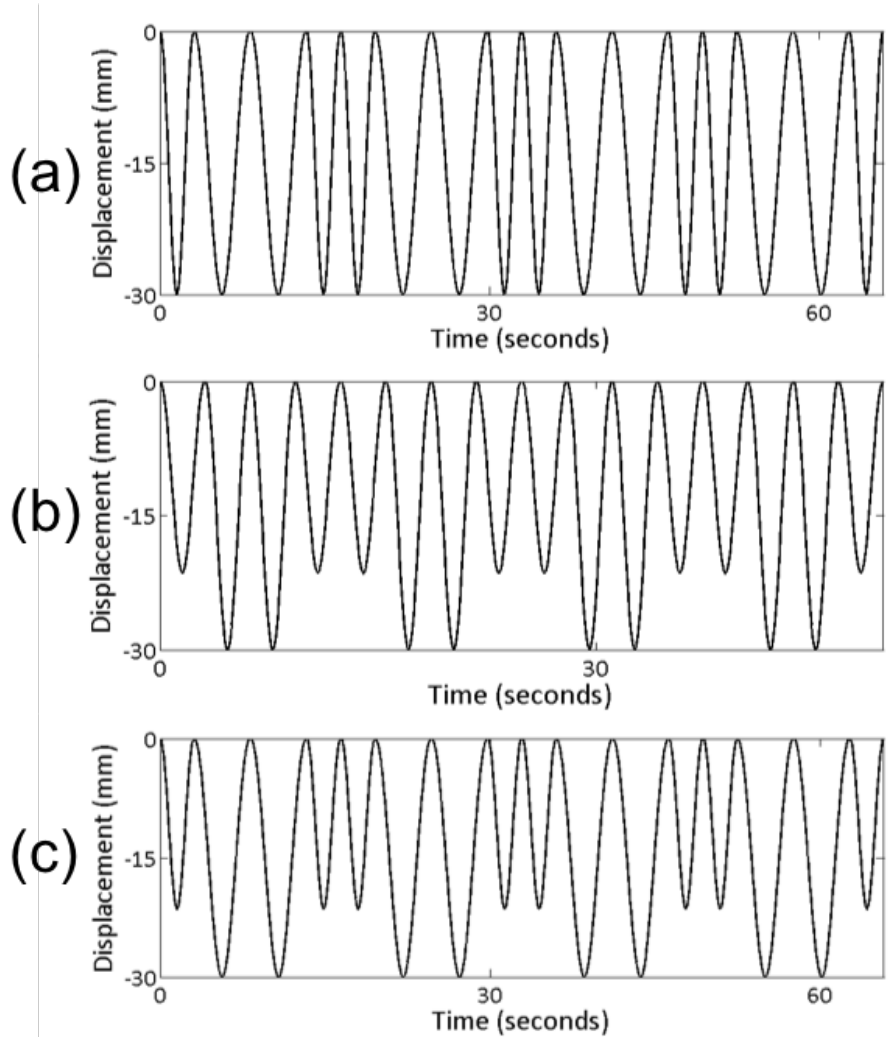

Figure 9: Simulated irregular breathing curves used for raw MRI data simulation: (a)cosine curve with changing period (b)cosine curve with changing amplitude (c)cosine curve with changing period and amplitude

(2) Patient irregular signals: Five patients' breathing signals acquired with the RPM system (Varian Medical Systems, Palo Alto, CA) are used to simulate the cine and sequential scans in the XCAT digital phantom. These signals are preprocessed to remove

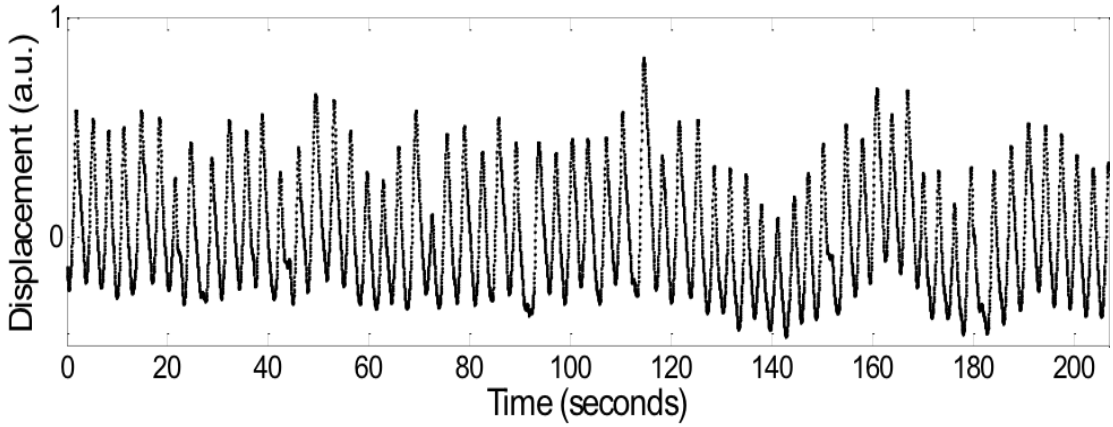

Figure 10: One of the irregular patient breathing curves used for raw MRI data simulation

some extreme peaks and valleys before using for scan simulation. One example of a patient breathing signal is shown in Figure 10.

2.3 Evaluation Methods

Three metrics were implemented to further evaluate the performance of this anatomic matching based sorting method regarding both the whole 4D image accuracy and tumor volume accuracy.

2.3.1 Total Relative Error

Total relative error (TRE) measures the relative difference between the reconstructed image and the ground truth image over the whole 4D volume. If two images are identical, the TRE will be 1. TRE can be calculated by the formula below:

$$TRE = \frac{\sqrt{(f - f_{GT})^2}}{\sqrt{f_{GT}^2}} \times 100\% \quad , \qquad [5]$$

where f is the reconstructed 4D image and f_{GT} is the ground truth image.

2.3.2 Volume-Percent-Difference

Tumors in the images were automatically contoured by a Matlab program. Then the Volume-Percent-Difference (VPD) metric is utilized to estimate the accuracy of tumor volume in the 4D images compared with the ground truth images. VPD can be calculated by the formula follows:

$$VPD = \frac{|V \cup V_0 - V \cap V_0|}{V_0} \times 100\% \quad , \qquad [6]$$

where V_0 is the tumor volume in the ground truth image and V is the tumor volume in the reconstructed 4D images. VPD will be 0 if the two 4D images sets are identical.

2.3.3 Center-of-Mass-Shift

Center-of-Mass-Shift (COMS) represents the shift of the tumor center; ideally it will become 1 when the reconstructed image perfectly is matched with the ground truth. It can be estimated by the formula below:

$$COMS = \sqrt{\Delta x^2 + \Delta y^2 + \Delta z^2} \quad , \qquad [7]$$

where Δx, Δy and Δx is the center-of-mass distance from the tumor volume in 4D image to the tumor in the ground truth.

3. Result

3.1 Aim 1 Result

Figure 11 shows the result of the 4D images generated by the anatomic feature matching-based method, as compared to the conventional phase sorting (PhaseS) method and the ground truth images in both cine and sequential acquisition modes with a regular cosine breathing pattern. The subtraction of the reconstructed 4D images by anatomic feature matching from the ground truth(GT) images, or the difference maps, are also generated for better visual evaluation. Only first five phases of the 4D image set including the end of exhalation(EOE) and end of inhalation(EOI) phases are displayed in the figure. The red dashed lines in Figure 11 are used to improve the respiratory motion visualization. 'AFM' represents the anatomic feature matching method in this figure. In the difference map, it can be found that the reconstructed images from the anatomic feature matching method matched well with the ground truth images with minimal artifacts. In the 30% phase bin, artifacts are visible in the heart region, which are indicated by the blue arrows. These artifacts are caused by the difference between the nonsynchronous periods of heart motion and respiratory motion, which is not the major consideration of this study. In the red box in the Figure 11, it can be observed that the images generated by anatomic feature matching method can preserve a clear and smooth diaphragm structure, while the diaphragm boundary is blurred in the phase sorting method. The red arrows in the Figure 11 also indicate the tumor volume

comparison. The result of both cine and sequential acquisitions showed good consistency with the ground truth.

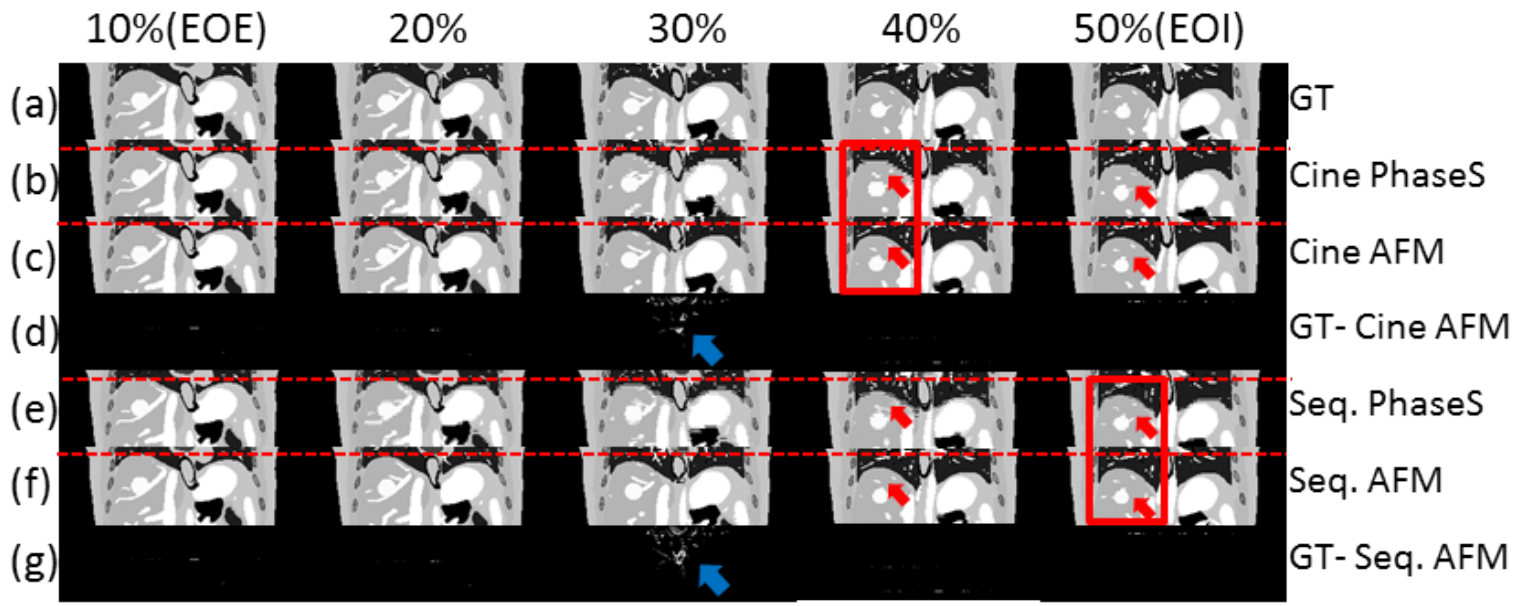

Figure 11: For regular breathing pattern: (a) The ground truth(GT) image in first 5 phases. (b) Phase sorting result of cine acquisition. (c) Anatomic feature matching-based(AFM) sorting result of cine acquisition. (d) Difference map between the GT and the AFM sorting result in cine mode. (e)Phase sorting result of sequential acquisition. (f)AFM sorting result of sequential acquisition. (g) Difference map between the GT and the AFM sorting result in sequential mode

3.2 Aim 2 Result

Figure 12 shows the result of the anatomic feature matching-based sorting method of one example simulated cosine-based irregular signal with changing period and amplitude, compared with the conventional phase sorting method and the ground truth images in both cine and sequential acquisition modes. Figure 13 shows the result of the anatomic feature matching-based sorting method of one example patient irregular breathing signal compared with the conventional phase sorting method and the ground truth images in both cine and sequential acquisition modes. As is indicated in the difference maps between the sorted images and the ground truth, the anatomic feature matching-based sorting method can generate 4D MRI images with minimal artifacts. Compared with the results of conventional phase sorting, this method can provide better anatomic structure consistency. It can be found from the red boxes and red arrows in the figures that the artifacts in the phase sorting result are more obvious as truncated diaphragm boundary and distorted tumor shapes compared with the proposed method. This improvement made by the anatomic feature matching method is strengthened with larger irregularity of the breathing pattern, which can be observed by comparing the results in Figure 12 and Figure 13. In addition, both the cine and sequential acquisition modes showed promising results with the anatomic feature matching-based 4D-MRI sorting method in irregular breathing.

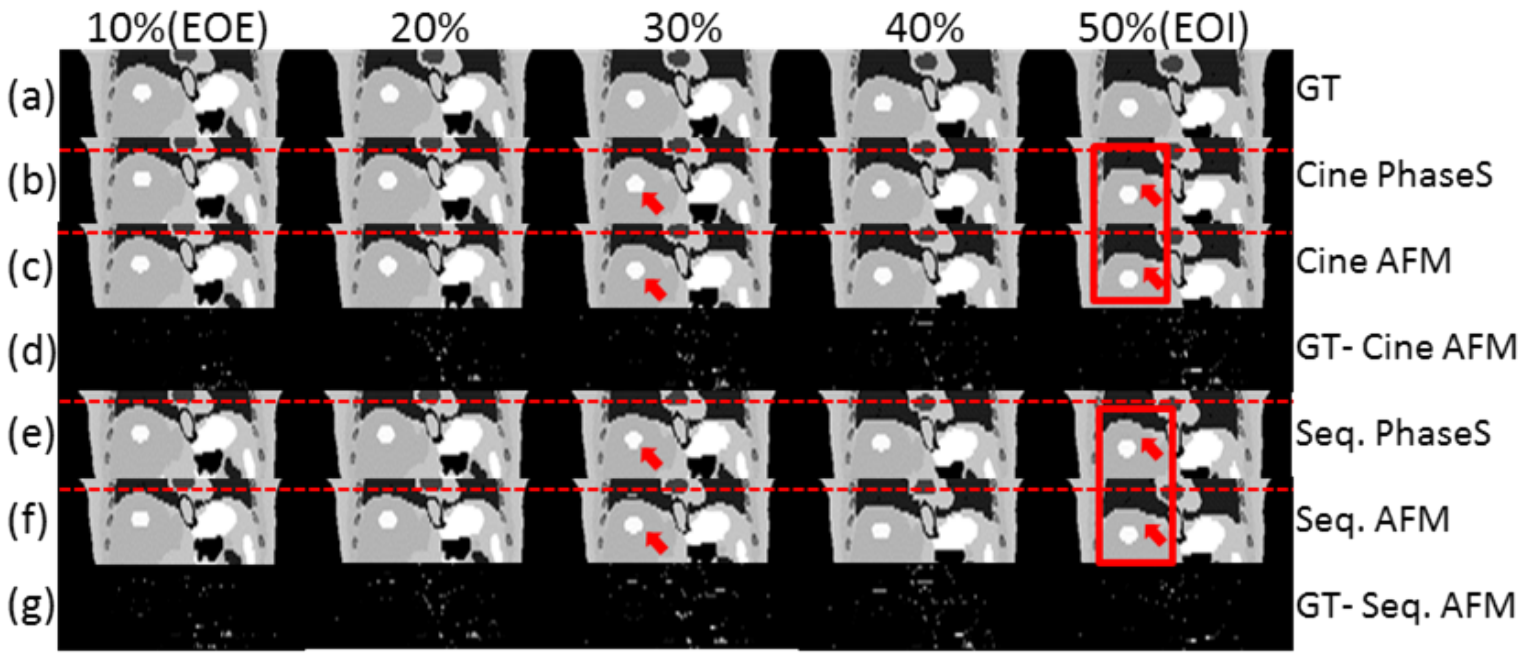

Figure 12: For simulated irregular breathing with changing period and amplitude: (a) The GT 4D image in first 5 phases. (b)Phase sorting result of cine acquisition. (c) AFM sorting result of cine acquisition. (d) Difference map between the GT and the AFM sorting result in cine mode. (e) Phase sorting result of sequential acquisition. (f) AFM sorting result of sequential acquisition. (g) Difference map between the GT and the AFM sorting result in sequential mode.

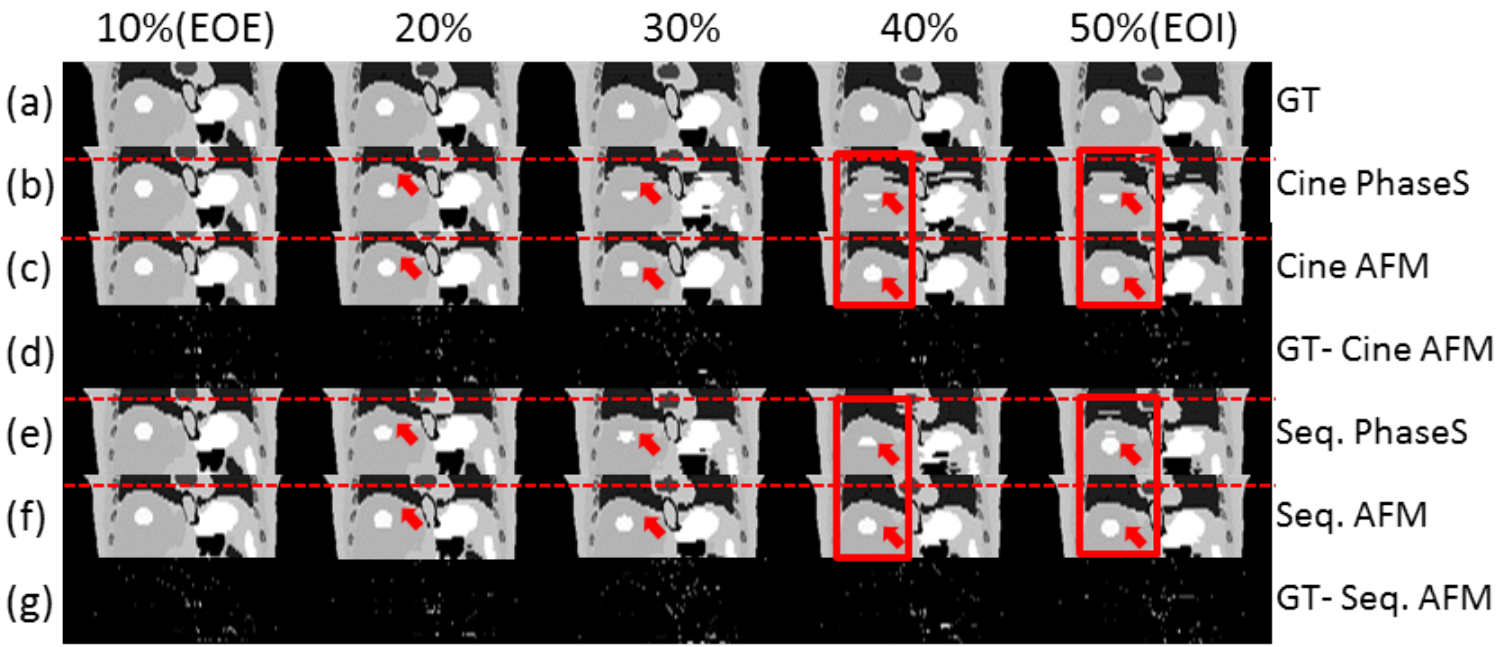

Figure 13: For patient irregular breathing signal #1: (a) The GT 4D image in first 5 phases. (b) Phase sorting result of cine acquisition. (c) AFM sorting result of cine acquisition. (d) Difference map between the GT and the AFM sorting result in cine mode. (e) Phase sorting result of sequential acquisition. (f) AFM sorting result of sequential acquisition. (g) Difference map between the GT and the AFM sorting result in sequential mode

Table 1: Regular breathing result evaluation

Case	TRE	VPD	COMS
Cine	0.28%	1.16%	0.06mm
Sequential	0.35%	1.23%	0.04mm
Mean_AFM	0.32%	1.20%	0.05mm
Mean_PhaseS	0.77%	1.87%	0.10mm

Table 2: Simulated irregular breathing result evaluation

Case#		TRE	VPD	COMS
Cine	Prd	0.79 %	4.19%	0.19mm
	Amp	1.09 %	4.98%	0.21mm
	PrdAmp	0.93 %	6.51%	0.31mm
	Mean	0.93%	5.23%	0.24mm
Seq.	Prd	1.22 %	4.91%	0.30mm
	Amp	1.39 %	5.93%	0.31mm
	PrdAmp	1.39 %	7.37%	0.36mm
	Mean	1.33%	6.07%	0.32mm
Mean_AFM		1.02%	5.65%	0.28mm
Mean_PhaseS		1.13%	10.47%	0.49mm

In Tabe 2, 'Prd' means the cosine-based breathing signal is changing in period only. 'Amp' means the cosine-based breathing signal is changing amplitude only. And 'PrdAmp' means the cosine-based breathing signal is changing in both period and amplitude.

Table 3: Patient irregular breathing result evaluation

Case#		TRE	VPD	COMS
Cine	1	0.97%	6.05%	0.50mm
	2	1.09%	5.89%	0.25mm
	3	1.26%	9.91%	0.36mm
	4	0.93%	5.37%	0.23mm
	5	1.03%	7.90%	0.28mm
	Mean	1.06%	7.02%	0.32mm
Seq.	1	1.10%	5.52%	0.10mm
	2	1.13%	8.05%	0.15mm
	3	1.27%	8.54%	0.53mm
	4	1.37%	7.58%	0.14mm
	5	1.17%	7.10%	0.18mm
	Mean	1.21%	7.36%	0.42mm
Mean_AFM		1.13%	4.26%	0.37mm
Mean_PhaseS		2.97%	25.85%	1.23mm

Table 1 shows the quantitative evaluation of the anatomic feature matching-based sorting method for both cine and sequential acquisition in regular breathing pattern, regarding the accuracy of whole 4D image volume and the estimated tumor volume in the 4D images. It can be indicated from this table that this anatomic feature matching-based sorting method can provide good tumor volume consistency on average with minimal 4D volume difference with the ground truth. Both cine and sequential modes can reconstruct 4D-MRI images with improved accuracy and clear organ/tissue structures with minimum mismatch.

Table 2 and Table 3 show the quantitative evaluation of the anatomic feature matching-based sorting method compared with the conventional phase sorting method for both cine and sequential acquisition in irregular breathing patterns, including simulated and patient breathing respectively, regarding the accuracy of whole 4D image volume intensity and the estimated tumor volume in the 4D images. It can be found from these tables that the anatomic featuring matching-based 4D-MRI sorting method can provide accurate volumetric information about the tumor and body compared with the conventional phase sorting results. The minimal values of TRE, VPD and COMS for this proposed method can indicate the reduced motion artifacts regarding the image quality. Besides, the values for the cine acquisition and sequential acquisition are very close in the implement of two different kinds of irregular breathing signals, which shows the feasibility of this sorting method in both MRI acquisition modes.

4. Discussion

4.1 Result Discussion

Breathing variation related artifacts are inherent in the conventional 4D MRI images, which can be shown as discontinuities in the organ structures. Different approaches have been developed to reduce this motion artifact. For instance, Hu et al. [16] developed a prospective 4D-MRI technique to implement an amplitude-based gating system to avoid the imaging during the irregular breathing patterns. Liang et al. [33] developed a retrospective 4D-MRI sorting method as probability-based multi-cycle sorting to incorporate breathing variation information in the sorting process to reduce the related artifacts. But due to the sorting scheme, this probability-based multi-cycle sorting cannot be applied in cine acquisition, which will limit the choices of imaging sequences and the related contrast selection.

In this study, a robust 4D-MRI sorting method based on anatomic feature matching was developed and investigated to largely reduce the breathing variation related artifacts due to another new approach, which is to directly preserve the organ/tissue structures by aligning or matching them in two group of orthogonal images. The methods mentioned above utilized external breathing signals to guide the sorting or reconstruction procedure, which requires additional synchronization and correlation of the scan and breathing signal. This new method utilized the change of anatomic feature in images to form the bins and to guide the sorting process, which can

provide better validity and accuracy. In addition, some of the previous methods are only applicable in a specific data acquisition mode. However, for the anatomic feature matching method, it is feasible in both cine and sequential mode, which enables a wider choice of imaging sequences and contrasts.

As is shown in the results, the reconstructed 4D-MRI images are in great consistency with the ground truth and show substantially reduced motion artifacts and clearer organ structures compared with the conventional phase sorting method. This is more obvious in the patient breathing case, where the anatomic feature matching-based sorting method can still generate images with smooth organ structures and minimal artifacts, while the irregular breathing pattern strongly influences the performance of phase sorting method. The artifacts are more likely to be found in the EOI phase in the reconstructed images, while the EOE phase images show better consistency with the ground truth. This is consistent with the fact that EOI is the less stable phase in a breathing cycle and EOE is the more stable phase. It can also be found from the quantitative analysis that this new sorting method can provide good overall volumetric accuracy with only 1.13% total relative error, and as small as 7.19% volume difference and 0.37mm center-of-mass shift for the target volume, which is greatly improved compared with the conventional method.

In addition, from Tables 1-3 it can be found that the result of cine acquisition provides slightly better consistency with the ground truth than the result of the

sequential acquisition. This is potentially due to the different scanning strategies of these two scan modes. All the simulated scans have the same number of scan repetitions; that is, 20 times. For the cine acquisition, it continuously obtains images at one slice position over several breathing cycles to provide continuous diaphragm motion. However, for the sequential acquisition which acquire images slice location by slice location, this process is more random, and it is harder to predict the completeness for the slices to fill all the phase bins.

4.2 Limitation

First of all, this 4D-MRI sorting method based on anatomic feature matching is only tested on the XCAT digital phantom. Only 5 clinical patient breathing signals were utilized to simulate the raw MRI data. Further investigation using more patient breathing signals are need to analysis the significance of this new sorting method. Besides, only the diaphragm extraction part has been practiced on real patient images so far. The performance of this method in patient image data needs to be further tested to evaluate its robustness and accuracy in different patient scenarios.

The patient breathing data used in this study was preprocessed to eliminate some extreme peaks and valleys that might be caused by coughing or other large motion during the acquisition. Thus, the simulation process only simulates images under free breathing without extreme irregularity. Since the 2D images are sorted by matching anatomic feature from the images of an averaged breathing curve. The presence of

coughing and large motion can cause insufficient useful data and might further cause empty phase bins. The influence of the extreme irregularity can be investigated by adding large peaks and valleys in the breathing signal in simulation.

In addition, the current diaphragm extraction methods still need manual operation in the very first step. It needs to be further automated to improve the robustness and operation speed, with a goal of full automation. The simulated MRI images generated from XCAT have good pixel intensity contrast, which makes the diaphragm extraction less sensitive to the noise and resolution limitation. Therefore, this extraction method need to be further improved to provide more accurate results in the patient image, which has higher noise and more complicated pixel intensity shifts.

Another limitation of this study is that this sorting method can only work for the axial slices which contain the diaphragm structure. For real patient data with larger slice thickness, the number of slice positions that meet this requirement might be limited. Smaller slice thickness allows more slices within the diaphragm region, but can be more sensitive to the breathing irregularity, and it needs more time in the acquisition. Larger slices thickness can shorten the acquisition time and make the sorting process less sensitive to the irregularity, however, it will limit the resolution and number of slices to cover the diaphragm. In this study, the slice thickness is set as 0.5cm, which is common in the 4D-MRI scans. To sort other axial slices outside the diaphragm region, this method needs to be hybridized with other 4D-MRI sorting methods, or to utilize other

anatomic features to generate the 4D-MRI volume for the whole abdominal region. Other possible anatomic landmarks like the body surface, lung boundary and other large-contrast edges can be investigated in the future to test the feasibility.

5. Conclusion

A 4D-MRI technique based on anatomic feature matching has been developed and evaluated in a digital phantom. It utilizes the diaphragm structure as the landmark feature in two groups of orthogonal images to guide the sorting process. This anatomic feature matching-based method is feasible and can be applied in both cine and sequential acquisition modes. In addition, it is less susceptible to breathing variations and can generate 4D-MRI images with significantly reduced motion artifacts. The simulation study results of patient irregular breathing signal matched well with the ground truth images qualitatively, and only have an average of 1.13% TRE, 7.19% VPD and $\pm$0.37mm COMS compared with the ground truth 4D volume quantitatively.

Future work needs to be done for further testing this method in patient image data, and to improve the diaphragm extraction method. More landmark features need to be discovered and incorporated to achieve the goal of 4D-MRI reconstruction of the entire abdominal region based on anatomic feature matching.

References

[1] Keall, P. J., Mageras, G. S., Balter, J. M., Emery, R. S., Forster, K. M., Jiang, S. B., ... & Ramsey, C. R. (2006). The management of respiratory motion in radiation oncology report of AAPM Task Group 76. Medical physics, 33(10), 3874-3900.

[2] Hugo, G. D., & Rosu, M. (2012). Advances in 4D radiation therapy for managing respiration: Part I–4D imaging. Zeitschrift für Medizinische Physik, 22(4), 258-271.

[3] Matney, J. E. (2013). Investigation of Respiratory Motion Management Techniques for Proton and Photon Radiotherapy of Lung Cancer.

[4] Benedict, S. H., Yenice, K. M., Followill, D., Galvin, J. M., Hinson, W., Kavanagh, B., ... & Purdie, T. (2010). Stereotactic body radiation therapy: the report of AAPM Task Group 101. Medical physics, 37(8), 4078-4101.

[5] Badawi, A. M., Weiss, E., Sleeman, W. C., Yan, C., & Hugo, G. D. (2010). Optimizing principal component models for representing interfraction variation in lung cancer radiotherapy. Medical physics, 37(9), 5080-5091.

[6] Heath, E., Tessier, F., & Kawrakow, I. (2011). Investigation of voxel warping and energy mapping approaches for fast 4D Monte Carlo dose calculations in deformed geometries using VMC++. Physics in Medicine & Biology, 56(16), 5187.

[7] Liu, H. H., Balter, P., Tutt, T., Choi, B., Zhang, J., Wang, C., ... & Starkschall, G. (2007). Assessing respiration-induced tumor motion and internal target volume using four-dimensional computed tomography for radiotherapy of lung cancer. International Journal of Radiation Oncology• Biology• Physics, 68(2), 531-540.

[8] Keall P. 4-dimensional computed tomography imaging and treatment planning. Semin. Radiat. Oncol. 14:81-90, 2004.

[9] Low, D. A., Nystrom, M., Kalinin, E., Parikh, P., Dempsey, J. F., Bradley, J. D., ... & Politte, D. G. (2003). A method for the reconstruction of four-dimensional synchronized CT scans acquired during free breathing. Medical physics, 30(6), 1254-1263.

[10] Li, H. S., Zhong, H., Kim, J., Glide-Hurst, C., Gulam, M., Nurushev, T. S., & Chetty, I. J. (2013). Direct dose mapping versus energy/mass transfer mapping for 4D dose accumulation: fundamental differences and dosimetric consequences. Physics in Medicine & Biology, 59(1), 173.

[11] Pan T. Comparison of helical and cine acquisitions for 4D-CT imaging with multislice CT. Med. Phys. 32:627-634, 2005.

[12] Fayad, H., Pan, T., François Clement, J., & Visvikis, D. (2011). Correlation of respiratory motion between external patient surface and internal anatomical landmarks. Medical physics, 38(6Part1), 3157-3164.

[14] von Siebenthal, M., Szekely, G., Gamper, U., Boesiger, P., Lomax, A., & Cattin, P. (2007). 4D MR imaging of respiratory organ motion and its variability. Physics in Medicine & Biology, 52(6), 1547.

[15] Hu, Y., Caruthers, S. D., Low, D. A., Parikh, P. J., & Mutic, S. (2013). Respiratory amplitude guided 4-dimensional magnetic resonance imaging. International Journal of Radiation Oncology• Biology• Physics, 86(1), 198-204.

[16] Dinkel, J., Hintze, C., Tetzlaff, R., Huber, P. E., Herfarth, K., Debus, J., ... & Thieke, C. (2009). 4D-MRI analysis of lung tumor motion in patients with hemidiaphragmatic paralysis. Radiotherapy and Oncology, 91(3), 449-454.

[17] Blackall, J. M., Ahmad, S., Miquel, M. E., McClelland, J. R., Landau, D. B., & Hawkes, D. J. (2006). MRI-based measurements of respiratory motion variability and assessment of imaging strategies for radiotherapy planning. Physics in Medicine & Biology, 51(17), 4147.

[18] Liu, Y., Yin, F. F., Chen, N. K., Chu, M. L., & Cai, J. (2015). Four-dimensional magnetic resonance imaging with retrospective k-space reordering: A feasibility study. Medical physics, 42(2), 534-541.

[19] Deng, Z., Pang, J., Yang, W., Yue, Y., Sharif, B., Tuli, R., ... & Fan, Z. (2016). Four-dimensional MRI using three-dimensional radial sampling with respiratory self-gating

to characterize temporal phase-resolved respiratory motion in the abdomen. Magnetic resonance in medicine, 75(4), 1574-1585.

[20] Kothary, N., Heit, J. J., Louie, J. D., Kuo, W. T., Loo Jr, B. W., Koong, A., ... & Hofmann, L. V. (2009). Safety and efficacy of percutaneous fiducial marker implantation for image-guided radiation therapy. Journal of Vascular and Interventional Radiology, 20(2), 235-239.

[21] Bhagat, N., Fidelman, N., Durack, J. C., Collins, J., Gordon, R. L., LaBerge, J. M., & Kerlan, R. K. (2010). Complications associated with the percutaneous insertion of fiducial markers in the thorax. Cardiovascular and interventional radiology, 33(6), 1186-1191.

[22] Cai, J., Chang, Z., Wang, Z., Paul Segars, W., & Yin, F. F. (2011). Four-dimensional magnetic resonance imaging (4D-MRI) using image-based respiratory surrogate: A feasibility study. Medical physics, 38(12), 6384-6394.

[23] Liu, Y., Yin, F. F., Czito, B. G., Bashir, M. R., Palta, M., & Cai, J. (2017). Retrospective four-dimensional magnetic resonance imaging with image-based respiratory surrogate: a sagittal–coronal–diaphragm point of intersection motion tracking method. Journal of Medical Imaging, 4(2), 024007.

[24] Liu, Y., Yin, F. F., Rhee, D., & Cai, J. (2016). Accuracy of respiratory motion measurement of 4D-MRI: A comparison between cine and sequential acquisition. Medical physics, 43(1), 179-187.

[25] Liu, Y., Yin, F. F., Czito, B. G., Bashir, M. R., & Cai, J. (2015). T2-weighted four-dimensional magnetic resonance imaging with result-driven phase sorting. Medical physics, 42(8), 4460-4471.

[26] Tsunashima, Y., Sakae, T., Shioyama, Y., Kagei, K., Terunuma, T., Nohtomi, A., & Akine, Y. (2004). Correlation between the respiratory waveform measured using a respiratory sensor and 3D tumor motion in gated radiotherapy. International Journal of Radiation Oncology• Biology• Physics, 60(3), 951-958.

[27] Clements, N., Kron, T., Franich, R., Dunn, L., Roxby, P., Aarons, Y., ... & Ball, D. (2013). The effect of irregular breathing patterns on internal target volumes in four-dimensional CT and cone-beam CT images in the context of stereotactic lung radiotherapy. Medical physics, 40(2).

[28] Li, T., Thorndyke, B., Schreibmann, E., Yang, Y., & Xing, L. (2006). Model-based image reconstruction for four-dimensional PET. Medical physics, 33(5), 1288-1298.

[29] Rafael C.. Gonzalez, Richard E.. Woods, & Steven L.. Eddins. (2009). Digital Image Processing Using MATLAB®. Gatesmark Publishing.

[30] Otsu, N. (1979). A threshold selection method from gray-level histograms. IEEE transactions on systems, man, and cybernetics, 9(1), 62-66.

[31] Segars, W. P., Mahesh, M., Beck, T. J., Frey, E. C., & Tsui, B. M. (2008). Realistic CT simulation using the 4D XCAT phantom. Medical physics, 35(8), 3800-3808.

[32] Lee, D., Greer, P. B., Arm, J., Keall, P., & Kim, T. (2014). Audiovisual biofeedback improves image quality and reduces scan time for respiratory-gated 3D MRI. In Journal of Physics: Conference Series (Vol. 489, No. 1, p. 012033). IOP Publishing.

[33] Liang, X., Yin, F. F., Liu, Y., & Cai, J. (2016). A probability-based multi-cycle sorting method for 4D-MRI: A simulation study. Medical physics, 43(12), 6375-6385.